ANALYSIS OF WAVE-INDUCED ERRORS IN TURBULENT FLUX MEASUREMENTS

Gerald Karl Nifontoff

NAVAL POSTGRADUATE SCHOOL
Monterey, California

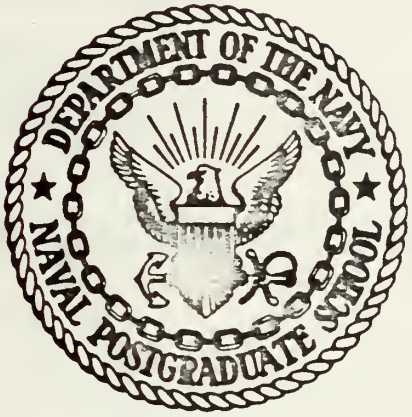

THESIS

ANALYSIS OF WAVE-INDUCED ERRORS IN

TURBULENT FLUX MEASUREMENTS

by

Gerald Karl Nifontoff

September, 1975

Thesis Advisor: Edward B. Thornton

Approved for public release; distribution unlimited.

SECURITY CLASSIFICATION OF THIS PAGE (When Data Entered)

REPORT DOCUMENTATION PAGE

READ INSTRUCTIONS BEFORE COMPLETING FORM

1. REPORT NUMBER

2. GOVT ACCESSION NO.

3. RECIPIENT'S CATALOG NUMBER

4. TITLE (and Subtitle)

Analysis of Wave-Induced Errors in Turbulent Flux Measurements

5. TYPE OF REPORT & PERIOD COVERED

Master's Thesis; September, 1975

6. PERFORMING ORG. REPORT NUMBER

7. AUTHOR(s)

Gerald Karl Nifontoff

8. CONTRACT OR GRANT NUMBER(s)

9. PERFORMING ORGANIZATION NAME AND ADDRESS

Naval Postgraduate School
Monterey, California

10. PROGRAM ELEMENT, PROJECT, TASK AREA & WORK UNIT NUMBERS

11. CONTROLLING OFFICE NAME AND ADDRESS

Naval Postgraduate School
Monterey, California 93940

12. REPORT DATE

September, 1975

13. NUMBER OF PAGES

14. MONITORING AGENCY NAME & ADDRESS(if different from Controlling Office)

15. SECURITY CLASS. (of this report)

Unclassified

15a. DECLASSIFICATION/DOWNGRADING SCHEDULE

16. DISTRIBUTION STATEMENT (of this Report)

Approved for public release; distribution unlimited.

17. DISTRIBUTION STATEMENT (of the abstract entered in Block 20, if different from Report)

18. SUPPLEMENTARY NOTES

19. KEY WORDS (Continue on reverse side if necessary and identify by block number)

Turbulent Flux
Waves
Upper Ocean

20. ABSTRACT (Continue on reverse side if necessary and identify by block number)

Near surface measurements of turbulent temperature and velocity fluctuations in the ocean are obscured by relatively much larger ordered fluctuations due to surface gravity waves. Analysis of measured velocity signals in the near surface region indicated that the ratio of turbulent to wave-induced kinetic energy was consistently less than 10^{-1}. To a first approximation, wave-induced fluctuations should not contribute to turbulent

DD FORM 1 JAN 73 1473 EDITION OF 1 NOV 65 IS OBSOLETE
S/N 0102-014-6601 |
(Page 1)

SECURITY CLASSIFICATION OF THIS PAGE (When Data Entered)

transport. However, small instrument errors due to misalignment, phase response, or directional response may cause significant wave-induced error in direct flux measurements. The effect on turbulent flux measurements of misalignment of the velocity sensors was examined. It was found that misalignment resulted in apparent phase shifts in the measured wave-induced signals, causing erroneous contributions to the calculated flux. For alignment errors of 3.6°, the error in caluclated momentum and heat fluxes could have been up to 500% and 110%, respectively. Momentum flux measurements made in deep water (with respect to the length of surface waves) were found to be less sensitive to alignment errors. The errors in this case were functions of the alignment of the flowmeter axes with the predominant wave direction.

Analysis of Wave-Induced Errors in Turbulent Flux Measurements

by

Gerald Karl Nifontoff
Lieutenant, United States Navy
B.S.E.E., Rensselaer Polytechnic Institute, 1969

Submitted in partial fulfillment of the
requirements for the degree of

MASTER OF SCIENCE IN OCEANOGRAPHY

from the

NAVAL POSTGRADUATE SCHOOL
September 1975

ABSTRACT

Near surface measurements of turbulent temperature and velocity fluctuations in the ocean are obscured by relatively much larger ordered fluctuations due to surface gravity waves. Analysis of measured velocity signals in the near surface region indicated that the ratio of turbulent to wave-induced kinetic energy was consistently less than 10^{-1}. To a first approximation, wave-induced fluctuations should not contribute to turbulent transport. However, small instrument errors due to misalignment, phase response, or directional response may cause significant wave-induced error in direct flux measurements. The effect on turbulent flux measurements of misalignment of the velocity sensors was examined. It was found that misalignment resulted in apparent phase shifts in the measured wave-induced signals, causing erroneous contributions to the calculated flux. For alignment errors of 3.6°, the error in calculated momentum and heat fluxes could have been up to 500% abd 110%, respectively. Momentum flux measurements made in deep water (with respect to the length of surface waves) were found to be less sensitive to alignment errors. The errors in this case were functions of the alignment of the flowmeter axes with the predominant wave direction.

TABLE OF CONTENTS

LIST OF TABLES

LIST OF FIGURES

I. INTRODUCTION

Turbulent processes in the upper ocean are not yet fully understood. Phillips (1966), Kitaigorodskii (1971) and others have pointed out the need for near surface measurements of turbulence and turbulent transfer. Large coordinated experiments such as BOMEX have been designed to measure turbulence in the Marine Boundary Layer of the atmosphere (Holland, 1972), but complementary measurements in the near surface layer of the ocean have been scarce. The recently completed GATE should greatly add to such data. Several projects (NORPAX, JASIN, GARP) are currently being planned to measure turbulence in what is generally termed the mixed layer of the ocean.

The dynamics of the near surface layer (in the absence of tropical storms) are dominated by surface gravity waves. The ordered motion of the waves is usually not of interest when making turbulence measurements because they do not contribute, at least to a first approximation, to the vertical transfer of heat and momentum through the water column. As a result, near surface turbulence measurements seek to resolve what are essentially second order quasi-random motions against a background of first order coherent noise.

The Naval Postgraduate School has conducted a series of turbulence measurements using a fixed array of sensors mounted on the Naval Undersea Center oceanographic research

tower off San Diego (Hagen, 1974). An attempt was made to measure turbulent heat and momentum fluxes from simultaneously recorded time series of orthogonal velocity components and temperature. It was found that wave-induced fluctuations may have caused significant errors in the measurements. In view of the current emphasis on near surface turbulence measurements, an analysis of wave-induced measurement errors was considered appropriate. Only through such analyses can realistic experiments be designed.

The analysis of wave-induced errors in turbulence measurement is carried out first, followed by a description of the experiment and the results obtained.

II. WAVES, TURBULENCE AND NOISE

In the upper layer of the ocean, turbulence is superimposed on ordered motions related to surface gravity waves. The contribution of the waves to a measured signal may be quite large. Data taken from the NPS experiments were examined as to the relative magnitudes of wave-induced signals, turbulence and noise. The data were presumed representative of open ocean as well as coastal near surface environments.

Fluctuations of horizontal and vertical velocity (u, w) and temperature, Θ, can be thought of as composed of wave-induced and turbulent parts:

$$\overline{u} = \overline{U} + \overline{u}'$$

$$w = W + w'$$

$$\theta = \Theta + \theta' \qquad (1)$$

where upper case letters stand for wave-induced fluctuations and primed letters for turbulent fluctuations. With certain assumptions it is possible to separate the wave-induced and turbulent parts of equation (1) and estimate their relative magnitudes. For moderate wave conditions, it is reasonable to assume that the wave-induced spectral velocity components can be calculated from the wave spectrum using linear wave theory. The success with which wave velocities are described by linear wave theory can be gauged by applying the appropriate linear transfer function to the surface displacement spectrum and studying how well the calculated and measured velocity spectra compare. Figure (1) shows the measured vertical velocity spectrum at 6.6 meters depth and that calculated from the surface displacement spectrum using linear wave theory. Figure 2 shows the coherence and phase functions obtained from the cross spectrum between measured wave and velocity records. The maximum coherency squared (hereafter referred to simply as the coherence) occurs at a period of 5.9 seconds and is equal to 0.9948. The phase function shows the waves leading the vertical velocities by approximately 90° throughout the surface wave band. Figures 1 and 2 clearly demonstrate the applicability of linear wave theory to wave-induced motions.

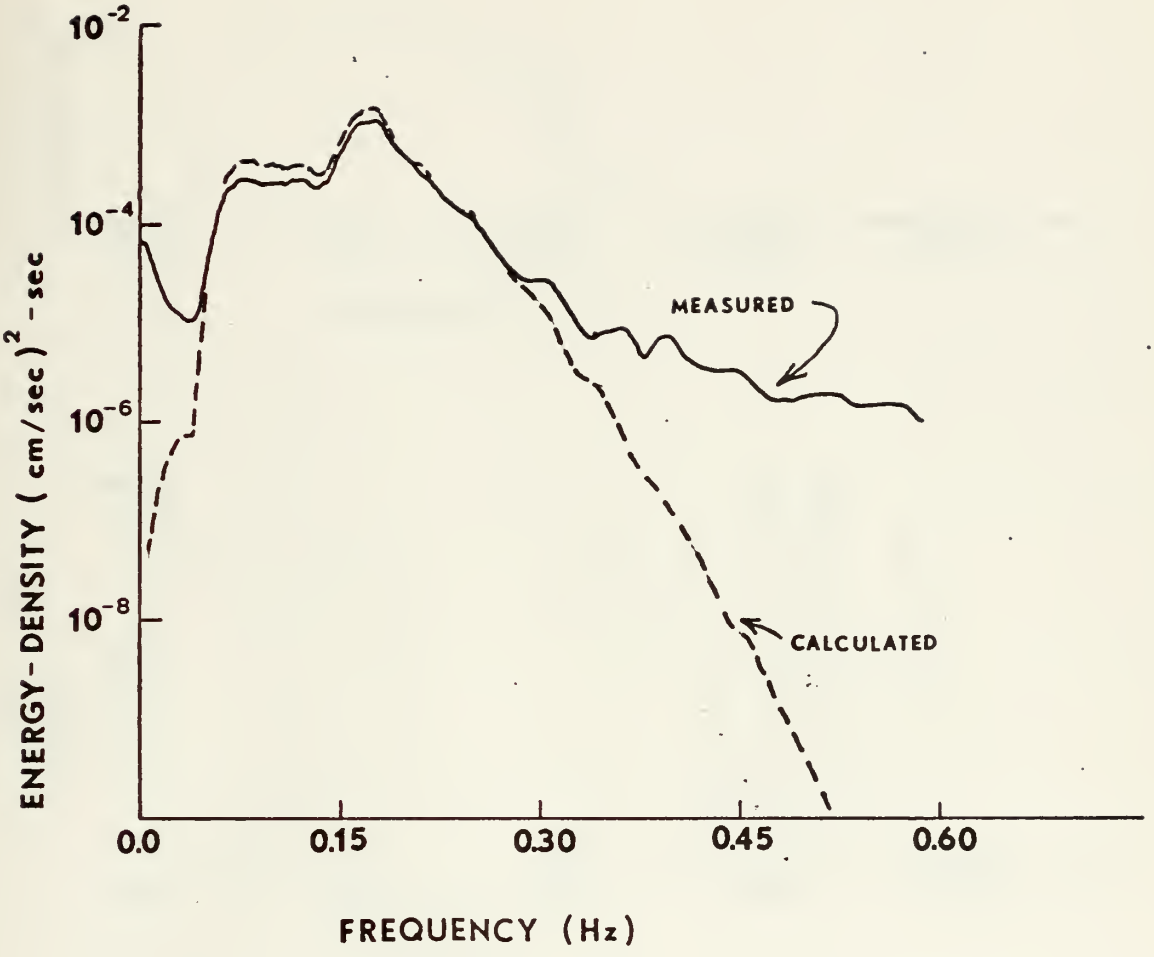

Figure 1. Comparison between measured vertical velocity spectrum and the vertical velocity spectrum calculated from the waves using linear theory.

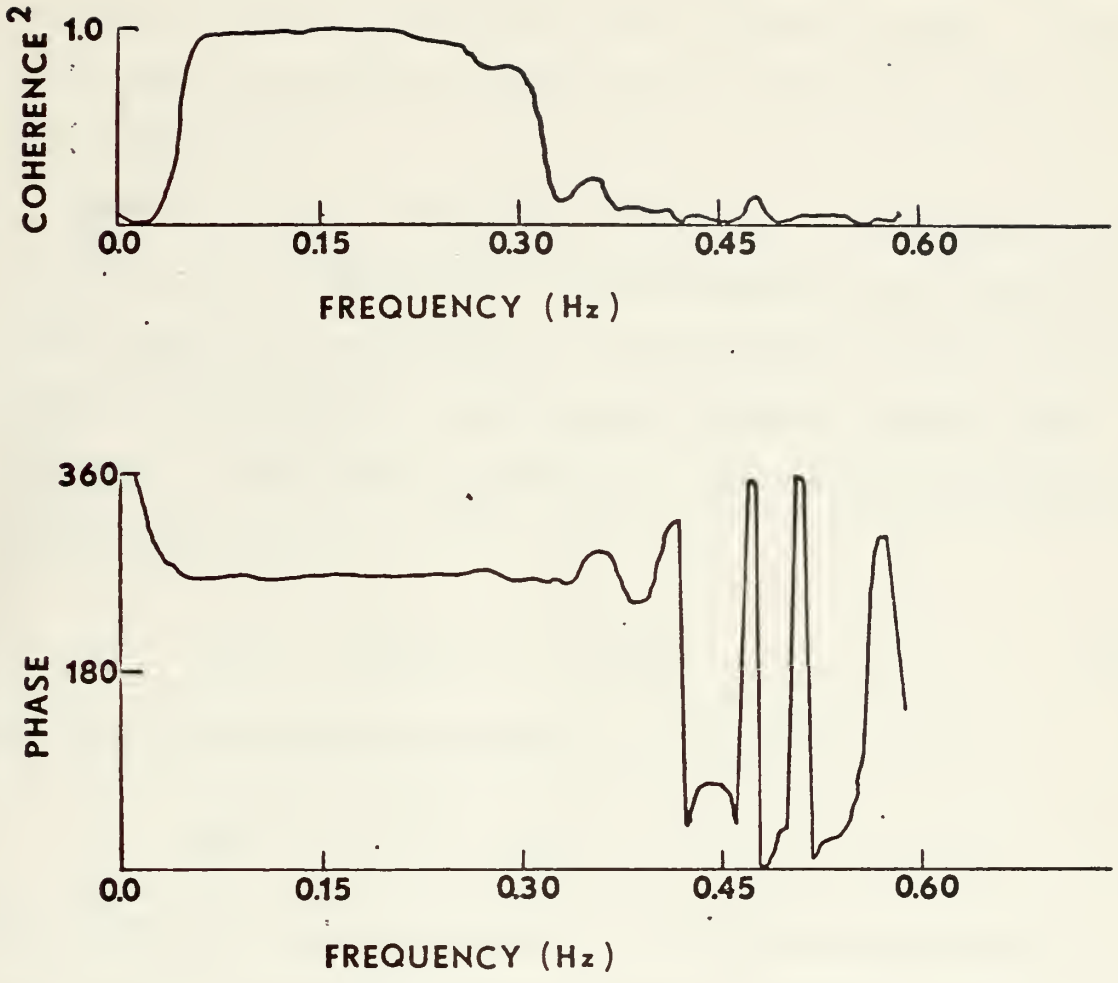

Figure 2. Coherence and phase functions calculated from the cross spectrum between surface displacement and vertical velocity.

It is assumed that wave-induced and turbulent motions are independent (Phillips, 1966) (Seitz, 1971). The interactions between wave motions and turbulence contribute to the motion only at the third order (Kinsman, 1965). Therefore, the independence assumption is justified except for very steep waves.

Using the two preceding assumptions, the measured velocity spectrum can be separated into wave-induced and turbulent parts using the experimentally determined coherence between the wave displacement and velocity signals (Benilov and Filyushkin, 1970, see Appendix A). The turbulence spectrum is then given by

$$S_{w'}(f) = S_w(f)(1 - \gamma^2_{\eta w}) \tag{2}$$

and the wave-induced spectrum by

$$S_W(f) = S_w(f) - S_{w'}(f). \tag{3}$$

The variance of velocity due to wave-induced or turbulent motions is obtained by summing their respective spectral components. Table 1 lists experimentally determined velocity variances from the NPS data. The horizontal wave velocities are larger than the vertical velocities due to the shallow water environment. The magnitude of horizontal "turbulent" variance may not all be attributable to turbulence due to the effect of directionality of horizontal wave motions on the coherence (Yefimov and Khristoforov, 1971). Table 1 indicates that the intensity of turbulent motions decreases

RUN	DEPTH	VELOCITY VARIANCE ($cm^2 sec^{-2}$)					
		$\overline{u}^2$	$\overline{w}^2$	$\overline{U}^2$	$\overline{W}^2$	$\overline{u}'^2$	$\overline{w}'^2$
17	8.04	176.6	28.5	168.4	25.5	7.7	2.9
18	12.54	228.7	14.0	208.2	12.4	20.2	1.6
19	9.44	229.6	35.6	210.5	33.1	18.6	2.4
22	6.62	310.9	157.7	296.0	150.8	14.2	6.5
26	5.84	577.9	306.2	555.8	294.1	20.7	11.3
28	10.95	161.1	11.8	152.2	11.1	8.5	0.7
28a	10.95	133.4	10.8	126.0	10.1	7.1	0.7

TABLE I. Velocity variance calculated from wave-induced and turbulent velocity spectra.

RUN	DEPTH	TEMPERATURE VARIANCE ($°C^2$)		
		$\overline{\theta}^2$	$\overline{\Theta}^2$	$\overline{\theta}^2$
17	7.98	0.0787	0.0115	0.0672
18	12.48	0.0552	0.0026	0.0526
19	9.38	0.0089	0.0016	0.0073
22	6.56	0.0192	0.0067	0.0125
26	5.78	0.0178	0.0051	0.0127
28	10.89	0.0126	0.0019	0.0107
28a	10.89	0.0485	0.0095	0.0390

TABLE II. Temperature variance calculated from wave-induced and turbulent temperature spectra.

with depth roughly as the intensity of the wave motions. The ratio of turbulent to wave-induced energy is seen to be consistently less than 10^{-1}.

An inseparable part of the turbulent variance is that due to instrument noise. The advertised broadband noise level for the flowmeters used (Marsh-McBirney Model 711) was 1.0 $cm^2 sec^{-2}$. The noise level was checked by recording the instrument output while the flowmeters were at rest in still water and was visually found to agree with that advertised. Additional noise can be introduced in the form of turbulence created by the obstruction of the flow field by the sensor. At the small velocities measured this effect can probably be ignored (NOIC, 1974).

Making the additional assumption that temperature can be treated as a passive scalar, the assumptions made with regard to velocity fluctuations should apply equally well to the wave-induced and turbulent temperature fluctuations of equation (1). The wave-induced temperature fluctuations can then be written in terms of the vertical displacement of some local temperature gradient relative to the point of measurement (Thornton and Boston, 1974):

$$\Theta = Z \frac{\partial \overline{\theta}o}{\partial z} = \frac{W}{i\sigma} \frac{\partial \overline{\theta}o}{\partial z} , \qquad (4)$$

where Z is the wave-induced vertical displacement and $\partial \overline{\theta}o/\partial z$ is the temperature gradient. Equation (4) implies that the coherence between Θ and the surface displacement

is 1.0 and that the method of Appendix A can be used to separate wave-induced and turbulent temperature components. Table 2 shows the wave-induced and turbulent temperature variances calculated from the NPS data.

III. APPLICABILITY OF TAYLORS HYPOTHESIS

An associated problem of turbulence measurements in the near surface layer, although not directly tied to flux measurements, deals with the applicability of Taylor's hypothesis. Experimental turbulence data is usually in the form of a time history of turbulent fluctuations measured at a point or with a towed sensor. The spectra calculated from such measurements are then defined in frequency space. Unfortunately the theoretical treatment of turbulence is usually confined to wave number space, so that a transformation is employed. Turbulent frequencies are not uniquely related to their wavenumber, as is the case for wave motions for which a dispersion relationship exists. Instead, use is made of Taylor's hypothesis, or the frozen turbulence approximation. Taylor's hypothesis states that if a sensor is moved rapidly enough through a turbulent field, the time dependent changes in the field are negligible, with the result that it is the spatial variations that are being measured. A transformation from time to space can therefore be made by substituting x/U for t, where U is the velocity of the sensor (Tennekes and Lumley, 1972). For fixed point measurements the transformation can still be made, providing

that the turbulent field is being swept by the sensor fast enough, as by a mean wind or current. The criterion for the applicability of Taylor's hypothesis is that the relative velocity of the sensor with respect to the fluid be much larger than the magnitude of turbulent velocity fluctuations:

$$\overline{u}' / U << 1.$$

Meteorologist never seem to have trouble making the transformation because mean wind speeds are on the order of meters per second while small scale turbulent fluctuations are on the order of centimeters per second. Mean flow velocities in the ocean are usually measured in centimeters per second, as are turbulent fluctuations. In the ocean it is necessary to verify whether or not Taylor's hypothesis is valid, or to tow the sensor through the water at a speed considered sufficient to satisfy the approximation. The latter method has been used most often to date.

Seitz (1971) and Bowden (1963) concluded Taylor's hypothesis was valid in a tidal estuary for frequencies down to 0.25 Hz when the mean convective velocity was on the order of 25 cm/sec^{-1}. The NPS experiment did not include a good measurement of mean velocity, but turbulent fluctuations were on the order of 0.3 cm sec^{-1} per spectral estimate (Δf = 0.0067 Hz). A mean velocity of only 3.0 cm sec^{-1} could conceivably be sufficient to satisfy Taylor's hypothesis in this case.

High mean velocities are seldom encountered in the open ocean. Even where surface currents may be large enough, the measuring platform usually moves with the current so that relative velocities might be negligible. In such cases, it is doubtful whether Taylor's hypothesis can be applied.

IV. THEORY OF TURBULENT FLUX MEASUREMENT

If the Navier-Stokes equation is rewritten using mean and fluctuating velocities and then time averaged, one of the resulting terms is the Reynold's stress tensor (Phillips, 1966):

$$- \rho \overline{u_i u_j}, \quad i, j = 1, 2, 3 \tag{5}$$

were u_i are velocity fluctuations and the overbar denotes a time average. The off diagonal terms ($i \neq j$), represent a turbulent transport of momentum and are covariances of orthogonal velocity fluctuation components. If the motion can be considered horizontally homogeneous, the downstream component of vertical momentum flux is given, in conventional notation, by

$$\overline{uw} = \frac{1}{T} \int_o^T u(t)w(t)\, dt, \tag{6}$$

An analogous expression for vertical heat flux can be derived from thermodynamic relations and is

$$\overline{\theta w} = \frac{1}{T} \int_o^T \theta(t)w(t)\, dt, \tag{7}$$

where θ represents a fluctuating temperature. The covariance between two fluctuating quantities can also be expressed (Bendat and Piersol, 1971)

$$\overline{uw} = R_{uw}(0) = 2 \int_0^\infty Co_{uw}(f)\, df \ , \qquad (8)$$

where $Co_{uw}(f)$ is the real (in phase) part of the u-w cross-spectrum. The spectral representation is the most popular because turbulence theory has envolved in the spectral domain. Experimental determination of heat and momentum flux can be made by recording fluctuating velocity components u and w, and temperature fluctuations, θ, at a point and calculating the covariance or cospectrum as above.

Alternate methods for estimating turbulent heat flux are the dissipation method used by Williams and Gibson (1974)[1] and the profile method. The latter is essentially an integration over time of an assumed equation of conservation for heat (Voskanyan, et. al., 1969)(Kaiser and Williams, 1974). Both these methods have the advantage that only temperature measurements are necessary, while the eddy correlation method discussed above requires simultaneous temperature and velocity measurements. An advantage of the eddy correlation method is that the kinematic regime associated with turbulent heat flux can be analyzed.

---

[1] Measures only the eddy diffusion coefficient for heat.

V. WAVE EFFECTS ON FLUX MEASUREMENT

The wave-induced contribution to velocity signals in the near surface region has been shown to be much larger than the turbulent contribution. The effect of wave motions on the measurement of turbulent flux is analyzed below.

The covariance between u and w in a region of wave influence, assuming turbulent and wave-induced motions are statistically independent, can be written:

$$\overline{uw} = \overline{UW} + \overline{u'w'}. \tag{9}$$

For simplicity, u refers to only one horizontal velocity component. The first term is the contribution of the wave-induced motions and the second the contribution due to correlated turbulent velocity fluctuations. A similar expansion into wave-induced and turbulent parts can be made for temperature and vertical velocity covariance:

$$\overline{\theta w} = \overline{\Theta W} + \overline{\theta' w'}, \tag{10}$$

Since it has been shown that linear wave theory closely approximates observed data, U and W, as well as Θ and W (equation 4) are in quadrature and their contributions to the respective covariances should be zero. In terms of the cross spectrum:

$$S_{uw}(f) = Co_{uw}(f) - iQ_{uw}(f), \tag{11}$$

wave motions should contribute only to the imaginary part,

Recalling the definition (8), equation (9) can be written

$$\overline{uw} = \mathrm{Re}\left[2\int_0^\infty S_{uw}(f)\, df\right] = \mathrm{Re}\left[\overline{u'w'} - i(\overline{U}\,\overline{W} + \delta)\right] , \quad (12)$$

The contribution of the wave motions appears only in the (imaginary) quadrature spectrum because U and W are 90° out of phase. The quadrature contribution of the turbulence (δ) will henceforth be neglected compared to $\overline{UW}$. The simple overbar denotes RMS units. If, for some reason, the measured phase between U and W should differ from 90° a component of one signal will appear in phase with the other and contribute to the cospectrum. Such a contribution results in an error in the calculated flux. This error might be ignored for small phase differences were it not for the fact that the wave-induced signal is so much larger than the turbulent signal.

Real phase shifts between U and W due to non-linear effects have been postulated. For example Yefimov and Khristoforov (1972) included viscosity effects in the equations of motion to show that a phase shift occurs at second order for steep waves. The phase shift attenuates rapidly with depth and increases with increasing frequency. Consistent frequency dependent phase shifts were conspicuously absent from even our shallowest velocity records in the entire wind wave range of frequencies (see for example figure 1).

Other than unknown higher order or weak nonlinear effects, the only cause for the phase between horizontal and vertical

wave-induced velocities to differ from 90° is measurement error in directional response, frequency response, or improper instrument orientation. Non ideal directional response will be examined first.

A. FLOWMETER DIRECTIONAL RESPONSE

Expressing the true harmonic velocity component as

$$V = |\overline{V}| \cos \sigma t \tag{12}$$

the ideal response of a vertically oriented flowmeter is pictured in polar and cartesian form in figure 3a. If the flowmeter response deviates from the cosine law, the measured signal will be in error by some amount $\varepsilon(\sigma t)$ which depends on the magnitude and phase (i.e. direction) of $\overline{V}$. The measured signal becomes

$$V^* = |V| \cos \sigma t + |V| \varepsilon(\sigma t). \tag{13}$$

$\varepsilon(\sigma t)$ must be periodic in σt and can thus be decomposed into Fourier components which are all harmonics of σ but are not necessarily in phase with $\overline{V}$.

$$\varepsilon(\sigma t) = \sum_{n=1}^{m} \varepsilon_n \cos(n\sigma t + \phi_n). \tag{14}$$

There are three forms in which the error can appear. First, ϕ_n can be zero by virtue of the fact that the flowmeter will not respond to motions perpendicular to its axis. The poor directional response of the flowmeter in this case has the effect of broadening the bandwidth of the measured velocity signal by inclusion of the harmonics of $\varepsilon(\sigma t)$.

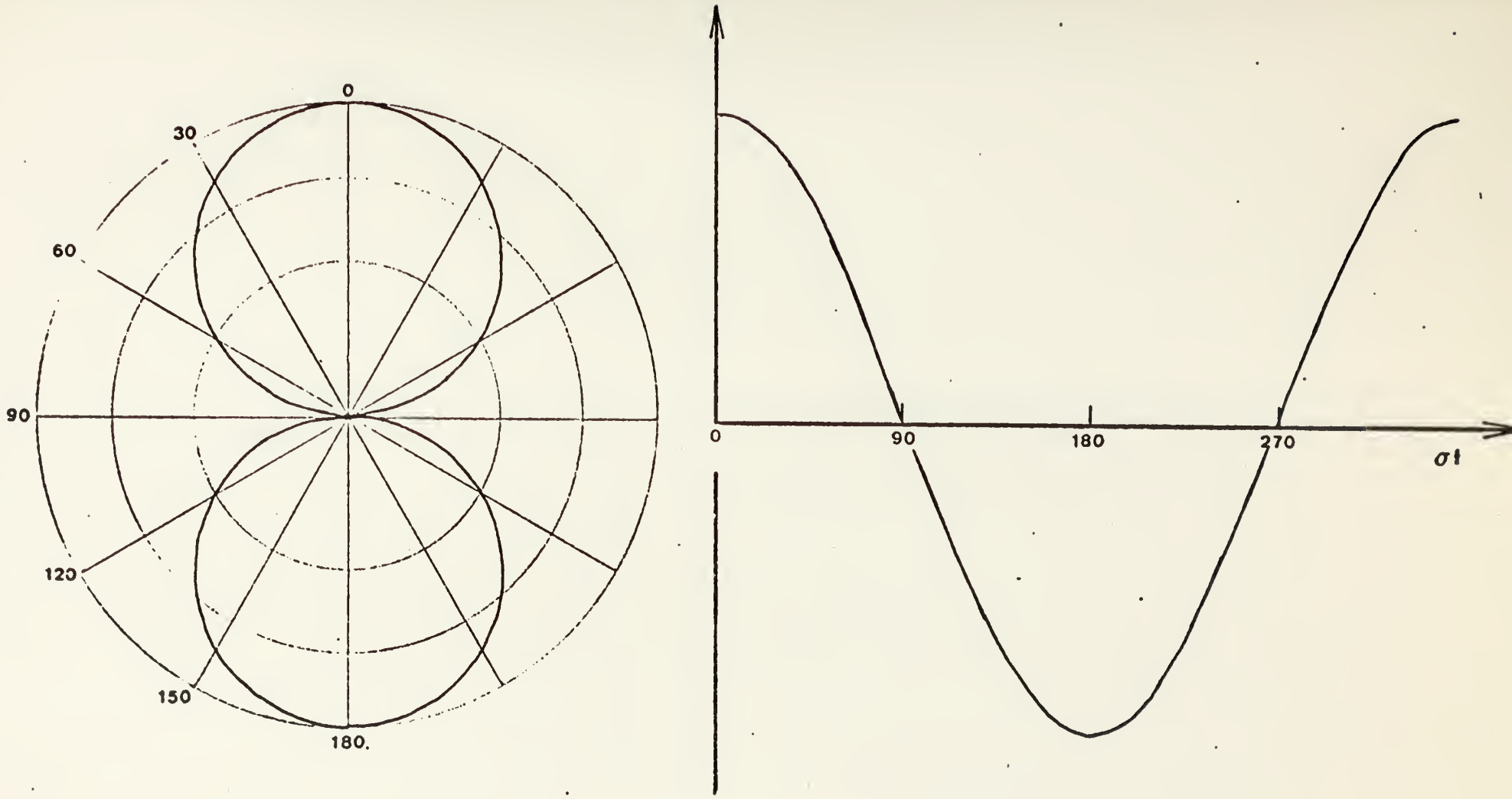

Figure 3a. Ideal Flowmeter Directional Response.

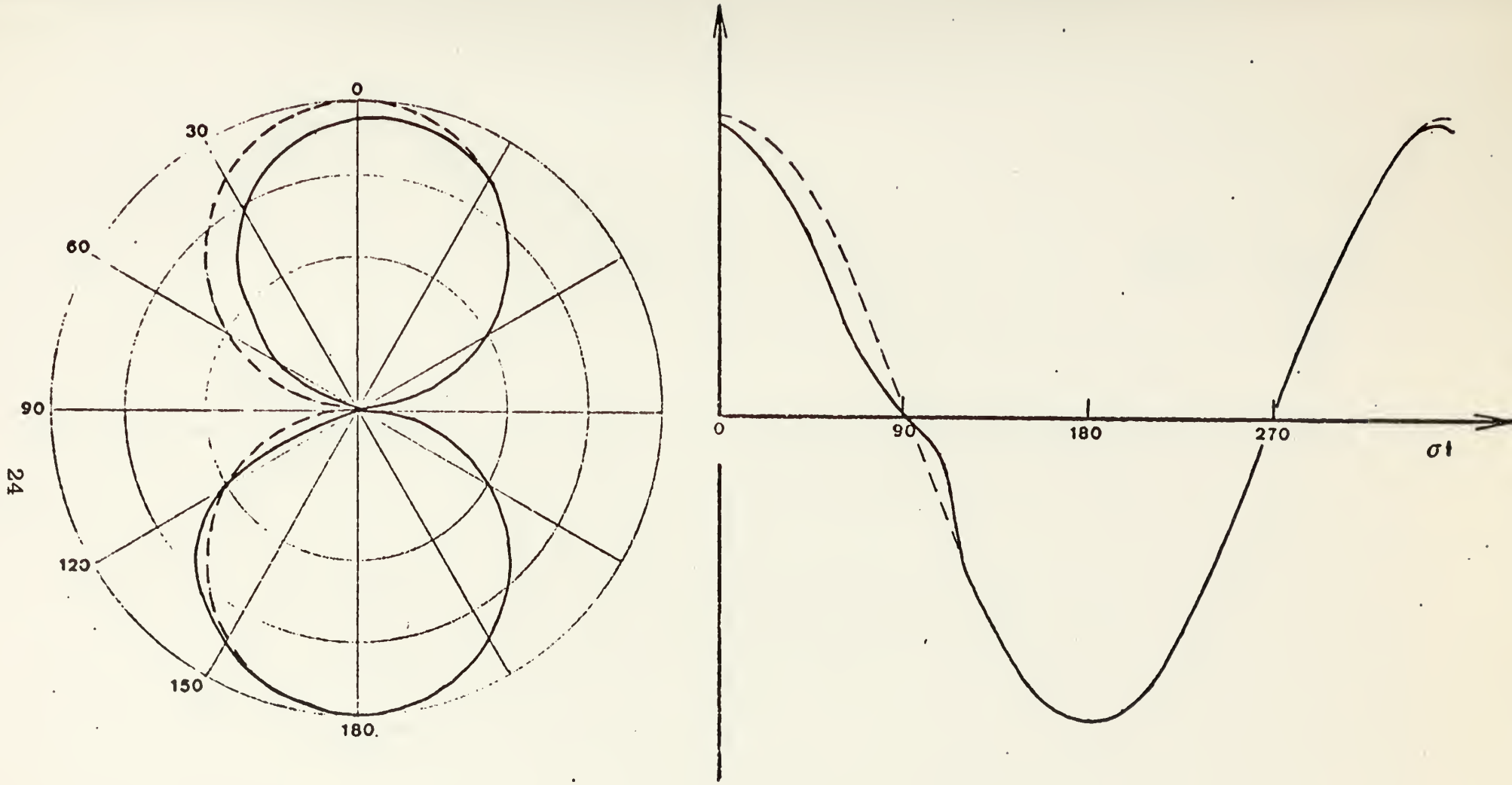

Figure 3b. Non-Ideal Flowmeter Response without Phase Error.

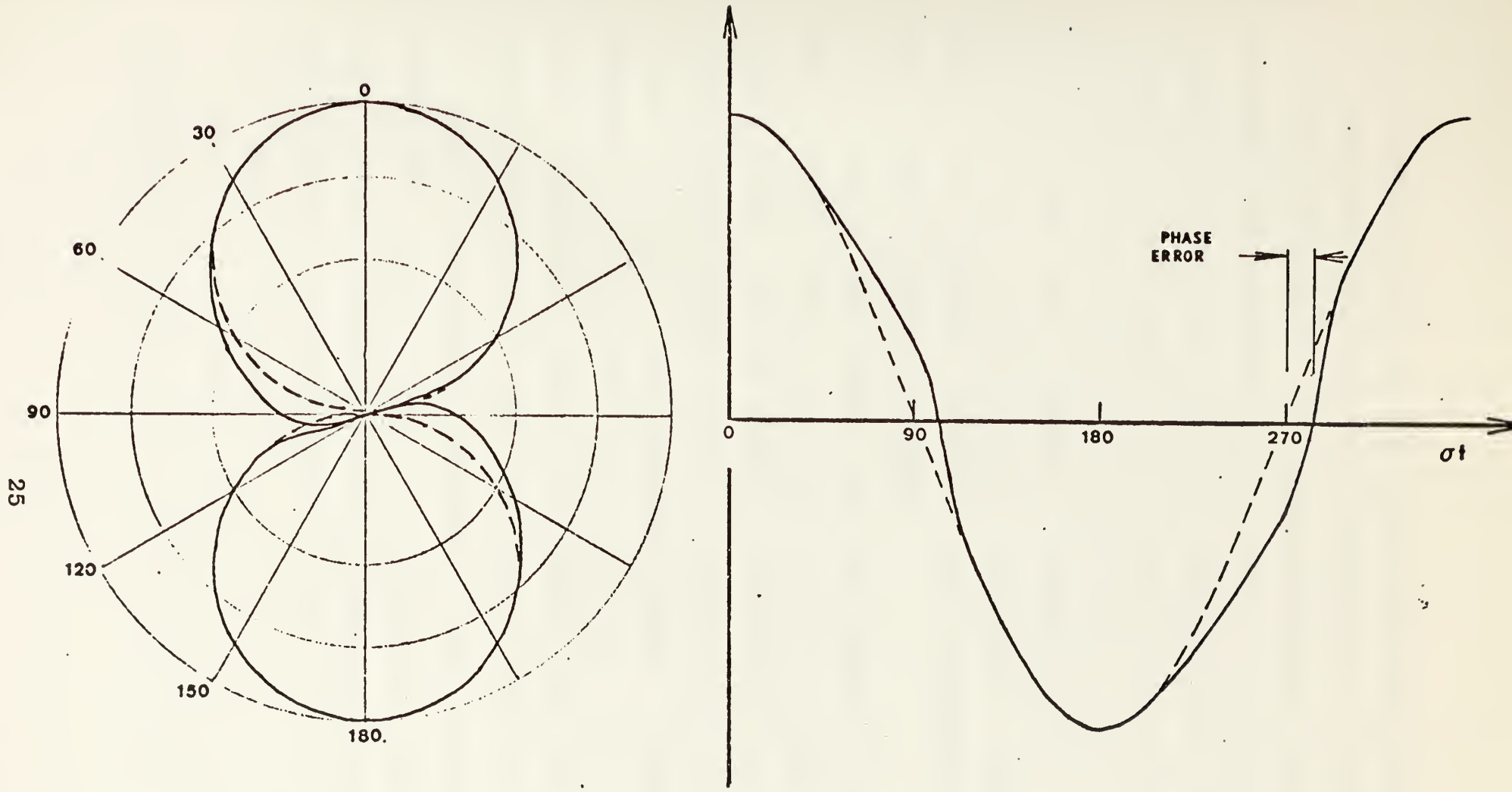

Figure 3c. Non-Ideal Flowmeter Response with Phase Error.

For flowmeters with noticeably poor directional response (as in figure 3b), this may create difficulties in analyzing velocity power spectra for slopes indicative of an inertial subrange above the wave frequency band. The electromagnetic flowmeters used here, and others tested by NOIC (1974), showed a typical first harmonic error response on the order of 2 to 4 percent of the ideal response amplitude. Table I indicates that the magnitude of turbulent fluctuations was on the order of 10 percent of the wave induced amplitudes. Contamination of the high frequency turbulent signal by harmonics of $\varepsilon(\sigma t)$ might therefore be possible.

As long as the flowmeter does not respond to perpendicular flow, however, the measured signal must be in phase with the actual motion. If, for example, the covariance is calculated between W* and another signal with which W should be in quadrature (say U), the two measured signals, including all harmonics of $\varepsilon(\sigma t)$, are still in quadrature. By virtue of their orthogonality there is no erroneous flux contribution. Surface waves usually occupy a frequency band of at least two octaves and there is a possibility that the first harmonic of the error signal in W* is not in quadrature with the U signal at that frequency. Since the phase between spectral wave components is random, however, the average contribution can be expected to be zero.

The second case of (14) is when the ϕ_n are zero but $\varepsilon(\pm \frac{n\pi}{2})$ is not because of a D.C. bias in the system. Errors

of this sort are inconsequential because D.C. values are normally subtracted out of the fluctuating signal before calculations are made.

The last schematic in figure 3 is for the case of $\phi_n \neq 0$. This kind of response occurs when the measured signal at $\sigma t = + \frac{\pi}{2}$ differs from that at $\sigma t = - \frac{\pi}{2}$. In other words, the meter response to a velocity component perpendicular to its axis depends on the direction of that velocity component. An error of this type does result in a phase shift of the measured signal with a consequent wave-induced contribution to the calculated covariance. Ducted type flowmeters in particular can respond erratically at very large angles of attack. Smith (1972) circumvented this difficulty by tilting his ducted impeller current meter array from the principal gravitational axis while measuring turbulent flux under Arctic ice. Unfortunately in the near surface region of the open ocean, the three dimensional wave motions have no preferred direction and this method does not work.

B. FLOWMETER FREQUENCY RESPONSE

There is an inherent phase lag in the response of any real sensor. Instruments for measuring turbulence are usually chosen to exhibit a flat amplitude response over the frequency band being measured. The phase response is seldom reported. Measurements using a variety of instruments, whose outputs are subsequently compared, are particularly susceptible to phase errors due to synchronization problems

and non-uniform phase response among the instruments. Later results will point out how extremely sensitive correlation measurements in the layer of wave influence are to miniscule errors in the measured phase. Care must be taken to ensure that all instruments have extremely short time constants or at least that the phase response of all instruments is the same.

C. FLOWMETER MISALIGNMENT

The other source of phase error in the measured velocity signals to be examined is that due to improper orientation of the velocity sensors with respect to the natural axes of wave motion. Since horizontal wave motions are directional, the orientation of the natural horizontal axes cannot be specified except that they are orthogonal to the local gravity vector. For each small band of the wave spectrum, however, it can be assumed that the direction is constant for a reasonable length of time. With this in mind, the three dimensional field of wave motions at a point can be represented by a Fourier sum of two dimensional motions, namely:

$$W = \sum_{n=1}^{m} |W_n| \cos(\sigma_n t + \phi_n)$$

$$U = \sum_{n=1}^{m} |U_n| \sin(\sigma_n t + \phi_n) \cos\beta_n \qquad (15)$$

$$V = \sum_{n=1}^{m} |U_n| \sin(\sigma_n t + \phi_n) \sin\beta_n$$

where β_n are the angles between the horizontal wave component directions and some arbitrary reference direction.

Choosing one Fourier component and setting β equal to zero allows the measurement of the motion to be simply analyzed by assuming that the flowmeter axes are in the plane of motion defined by U_n and W_n. Figure 4 shows the axes of the wave motion and two flowmeter component axes which are tilted by an arbitrary angle. From figure 4, the measured signals U_n^* and W_n^* are given by

$$U_n^* = |U_n| \sin\sigma t \cos\alpha_{11} + |W_n| \cos\sigma t \cos\alpha_{31}$$

$$W_n^* = |U_n| \sin\sigma t \cos\alpha_{13} + |W_n| \cos\sigma t \cos\alpha_{33} \quad . \tag{16}$$

The effect of misalignment of the velocity sensors on turbulent flux measurements can now be calculated by taking the covariance between U_n^* and W_n^* and Θ_n. Recognizing that Fourier wave components are independent, the covariances $\overline{U_n^* W_n^*}$ and $\overline{\Theta_n W_n^*}$ can be summed over all wave components to give the total covariance contribution for the entire wave spectrum (still assuming all $\beta_n = 0$). In terms of RMS amplitude this results in

$$\overline{U^* W^*} = \overline{U}^2 \cos\alpha_{11} \sin\alpha_{33} - \overline{W}^2 \cos\alpha_{33} \sin\alpha_{11} \tag{17}$$

$$\overline{\Theta W^*} = \overline{\Theta U} \sin\alpha_{33} \tag{18}$$

Equations (17) and (18) are the errors due to wave motion in measured turbulent flux if the flowmeter axes are misaligned.

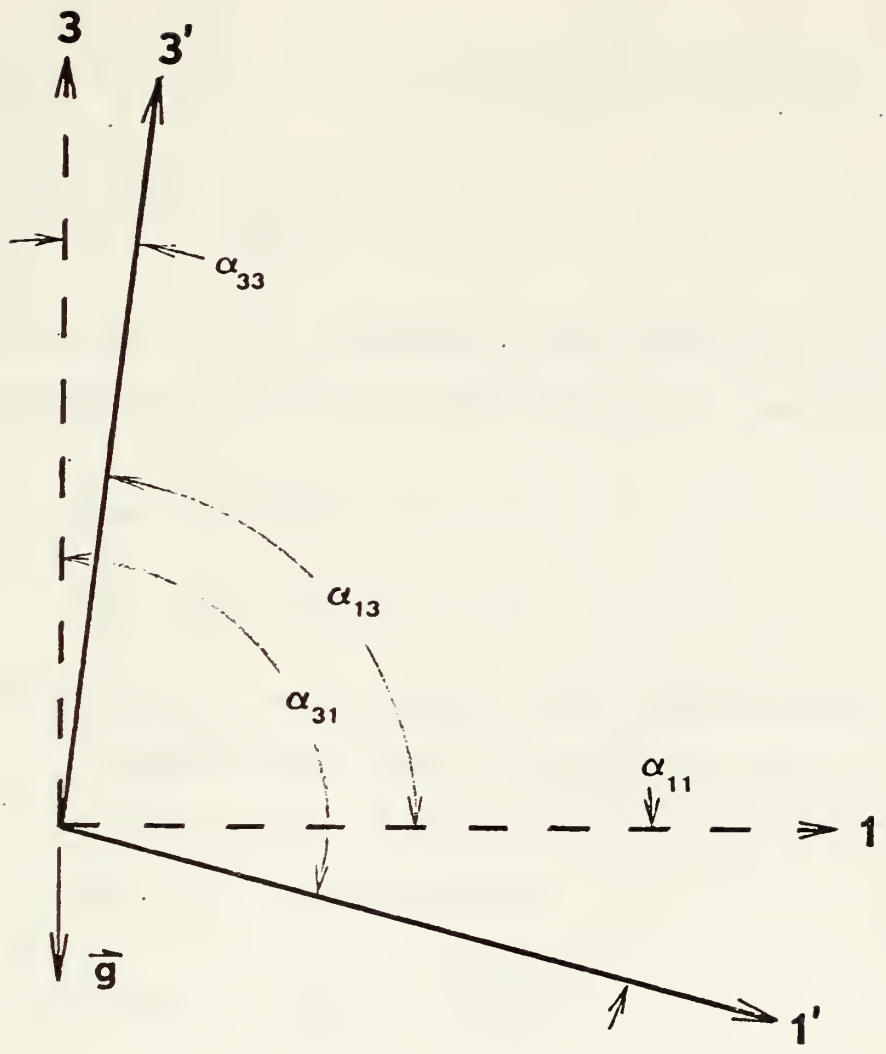

Figure 4. Measurement of two dimensional wave motion by flowmeter in the plane of motion. If the flowmeter axes are orthogonal: $\alpha_{11} = \alpha_{33}$, $\alpha_{31} = 90 + \alpha_{33}$, $\alpha_{13} = 90 - \alpha_{33}$.

From equations (9) and (10), the percent error introduced into the flux measurement is

$$\frac{\overline{u^*w^*} - \overline{u'w'}}{\overline{u'w'}} = \frac{\overline{U^*W^*}}{\overline{u'w'}} = \frac{\overline{U}^2 \cos_{11} \sin_{33} - \overline{W}^2 \cos_{33} \sin_{11}}{\overline{u'w'}} \qquad (19)$$

$$\frac{\overline{\theta w^*} - \overline{\theta' w'}}{\overline{\theta' w'}} = \frac{\overline{\theta U} \sin\alpha_{33}}{\overline{\theta' w'}} \qquad (20)$$

The true value of the turbulent covariance is not known, but the turbulence correlation coefficient (r') can be defined:

$$r'_{uw} = \overline{u'w'}/(\overline{u'}\ \overline{w'}) < 1 \qquad (21)$$

$$r'_{\theta w} = \overline{\theta' w'}/(\overline{\theta'}\ \overline{w'}) < 1 \qquad (22)$$

Dividing numerator and denominator of (19) and (20) by $\overline{u'}\ \overline{w'}$ or $\overline{\theta'}\ \overline{w'}$ as appropriate gives the percent error in terms of the tilt angles and the turbulence correlation coefficient. Equation (20), for example becomes

$$\text{Percent error} = \frac{\overline{\theta}\ \overline{U}}{\overline{\theta' w'}} \quad \frac{\sin\alpha_{33}}{r'_{\theta w}} . \qquad (23)$$

Equation (23) states that the percent error is inversely proportional to the "turbulent signal" to "wave-induced noise" ratio and the correlation between turbulent components. It is directly proportional to the tilt angle. Figure 5 shows the percent error (multiplied by the signal to noise ratio) for various values of the tilt angle and turbulence correlation coefficient.

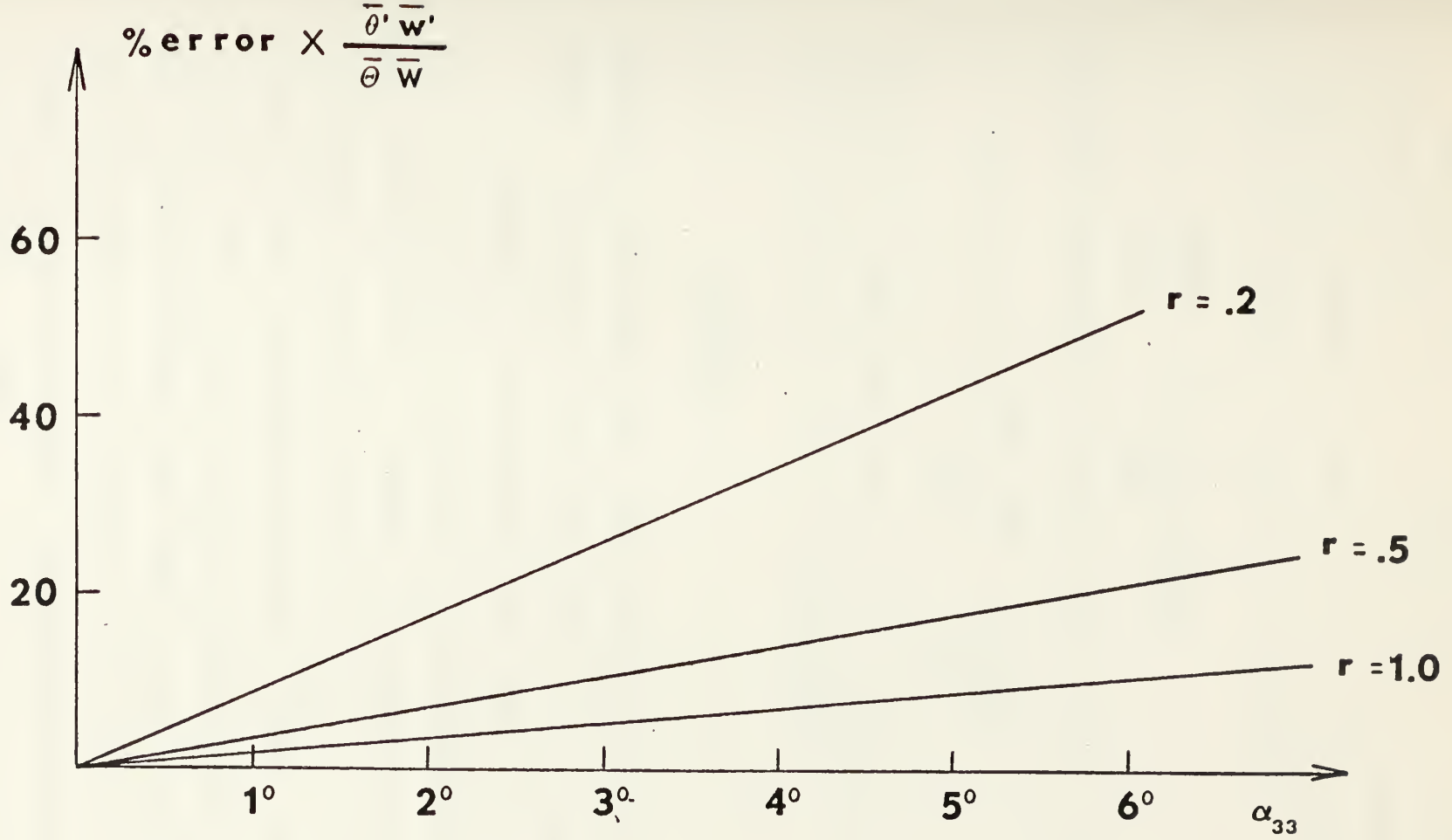

Figure 5. Turbulent Flux Error Due to Misalignment of Flowmeters.

Equation (19) can be simplified for illustrative purposes by assuming that the flowmeter axes are orthogonal so that $\alpha_{11} = \alpha_{33}$. Further assuming that the tilt angles are small, such that $\cos\alpha_{11} \approx 1$, equation (19) becomes

$$\frac{\overline{U^*W^*}}{\overline{u'w'}} = \frac{(\overline{U}^2 - \overline{W}^2)\ \sin\alpha_{33}}{\overline{u'w'}} \qquad (24)$$

and the expression for percent error can be written

$$\text{Percent error} = \frac{(\overline{U}^2 - \overline{W}^2)}{\overline{u}'\overline{w}'} \quad \frac{\sin\alpha_{33}}{r'_{uw}} \qquad (25)$$

Figure 5 is again applicable if the turbulent signal to wave-induced noise ratio is interpreted as

$$\frac{\overline{u}'\overline{w}'}{\overline{U}^2 - \overline{W}^2} \quad .$$

Equation (25) shows that, for the restricted case described above, the error in deep water (where W = U) should be zero.

An example of the momentum flux error can be calculated using the measured intensities of turbulent and wave-induced motions from Table 1. Assume a tilt angle of 5° and a turbulence correlation coefficient, r'_{uw}, of 0.2, which has been borrowed from Bowden and Howe's (1963) results in an estuary. The turbulent signal to wave-induced noise ratio for run 22 is obtained from Table 1 and is equal to 0.064. Entering figure 5, the product of the percent error and signal to noise ratio is 44. Solving for the percent error gives a value of 688%.

Since there are no representative values available for the correlation coefficient between turbulent temperature and vertical velocity fluctuations, estimates of the heat flux error rest on the assumption that $r'_{\theta w}$ is approximately equal to r'_{uw}. Using the previous values of 0.2 for $r'_{\theta w}$, 5° for the tilt angle, and the signal to noise ratio from Tables 1 and 2 (0.29) results in a percent error for the heat flux measurement of 155%. The heat flux measurement is less sensitive to tilt errors because of the larger signal to noise ratio.

The accuracy with which flowmeters must be aligned to achieve an acceptable percent error can also be calculated. For a 100% error, a signal to noise ratio of 0.064 and an assumed turbulence correlation coefficient of 0.2 the required alignment accuracy for momentum flux measurements is $\pm$ 0.73°. For the heat flux measurement, using the same values as the previous example, the required alignment accuracy is 3.3°.

For the general case where the horizontal axis of the flowmeter does not lie in the plane of all orbital motions (due to the directionality of the waves), the above development becomes more complicated. In this case, let the reference direction be the azimuth of the horizontal flowmeter axis so that β_n are the angles the horizontal wave motions make with the flowmeter axis, as in figure 6. With the coordinates defined as above all wave motions are in the 1-3 plane and V is zero for each individual spectral component. The response of the flowmeter to a typical wave field of

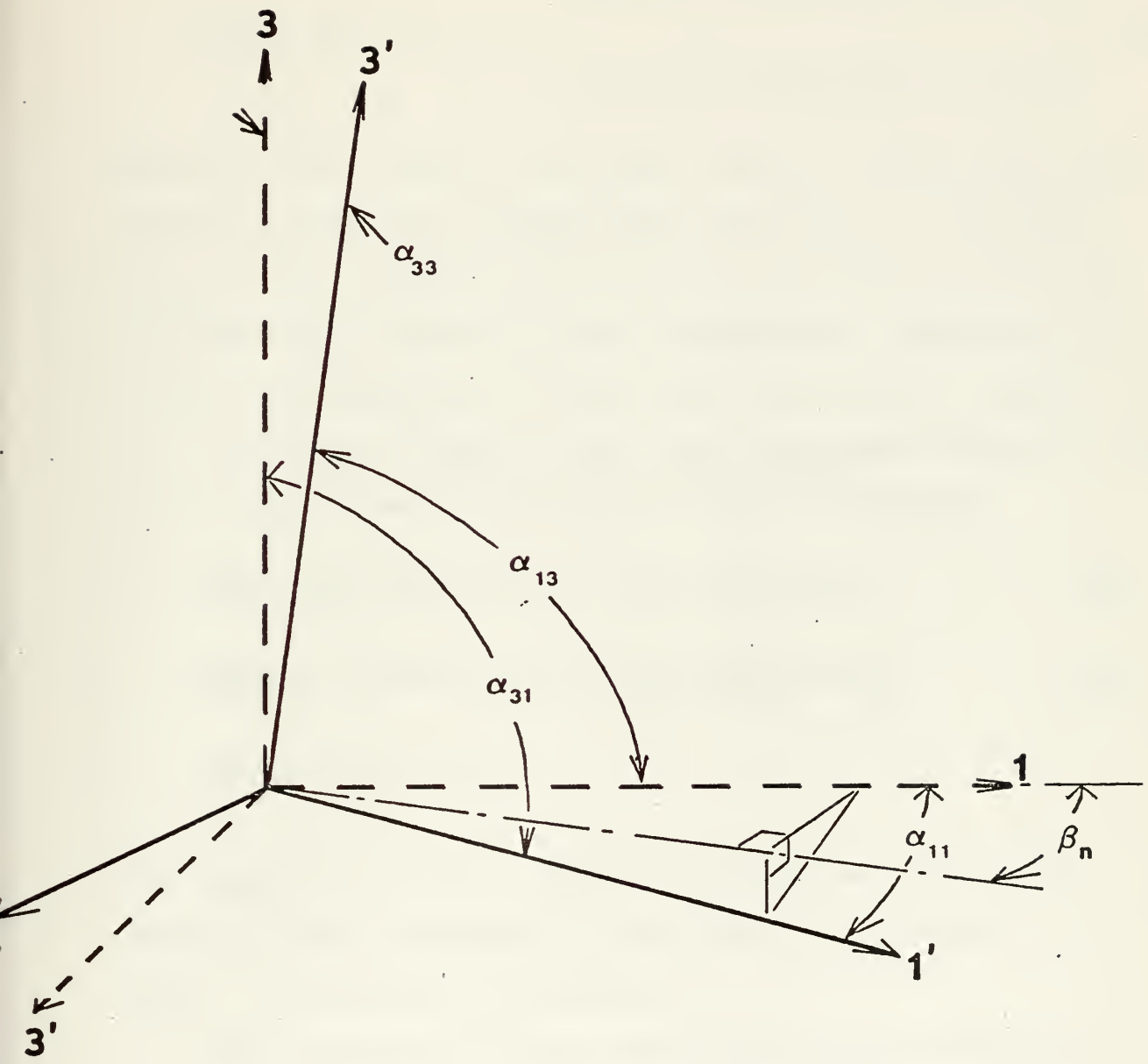

Figure 6. Measurement of Directional Two Dimensional Wave Motion by a Flowmeter not in the Plane of motion.

random direction is

$$(U_n^* \; V_n^* \; W_n^*) = (U_n \; W_n) \begin{pmatrix} \cos(\alpha_{11})_n & \cos(\alpha_{12})_n & \cos(\alpha_{13})_n \\ \cos(\alpha_{31})_n & \cos(\alpha_{32})_n & \cos(\alpha_{33})_n \end{pmatrix} \quad (28)$$

where the last term on the right consists of the directional cosines between the unprimed and primed axes. The angles $(\alpha_{ij})_n$ now include the effect of wave direction and may be different for different Fourier components. Considering a single wave component making an angle β_n with the azimuth of the horizontal flowmeter axis, the covariances between U_n^*, V_n^* and W_n^* and between Θ_n and W_n^* are easily calculated

$$\overline{U_n^* W_n^*} = U_n^2 \cos\alpha_{11}\cos\alpha_{13} - W_n^2 \cos\alpha_{31}\cos\alpha_{33} \quad (29)$$

$$\overline{V_n^* W_n^*} = -U_n^2 \cos\alpha_{12}\cos\alpha_{13} + W_n^2 \cos\alpha_{32}\cos\alpha_{33} \quad (30)$$

$$\overline{\Theta_n W_n^*} = \Theta_n \overline{U}_n \cos\alpha_{33}$$

The summation of wave components can not be accomplished, however, without knowledge of the direction spectrum of the waves. Even then it is difficult.

Again assuming that the flowmeter axes are orthogonal, some statements can be made about the wave-induced error. It is clear that the error contribution to the U_n^* signal is

$$W_n \sin(\alpha_{33})_n$$

regardless of the direction of the waves. On the other hand, the error contribution to W_n^* is a maximum at $\beta_n = 0$ (i.e.

when U_n is largest) and decreases as the quantity $\cos\beta_n$. The previous result for deep water thus does not hold and some error is to be expected in deep water flux measurements. The error for $\beta_n = 0$ in deep water is zero, as in equation (24). But the error for $\beta_n = 90°$ is a maximum given by

$$- W_n^2 \cos(\alpha_{33})_n \sin(\alpha_{33})_n, \tag{31}$$

since the U_n^* signal consists only of the W_n projection onto the 1' axis.

VI. DESCRIPTION OF THE EXPERIMENT

The Naval Postgraduate School (NPS) has conducted a series of turbulence measurements using a fixed array of sensors mounted on the NUC oceanographic research tower off San Diego. The array was designed to simultaneously measure surface elevation temperature, water particle velocity, conductivity and sound transmission parameters in a two cubic meter volume of ocean. A detailed description of the sensors and ancillary electronics was given by Hagen (1974). The data reported here consists of the output of a resistance wire wave gauge, a two-component electromagnetic flowmeter, and a thermistor adjacent to the flowmeter. The instruments were all mounted in a vertical line. The vertical separation between thermistor and flowmeter was six centimeters. Analog sensor outputs were recorded on FM multichannel tape recorders and subsequently passed through matched analog lowpass filters before being digitized. Prior to further

analysis, all records were highpass filtered using a running average filter with a 0.00675 Hz cutoff frequency to subtract out the low frequency fluctuations due to internal waves.

Data were obtained in water approximately twenty meters deep. A persistent thermocline was observed at mid-depth, the mean temperature profile being characterized by two nearly isothermal layers separated by a relatively sharp gradient. Figure 7 shows the position of the sensors in the water column and relative to the thermal structure as sampled by bathythermograph (Hagen, 1974). The thermocline was found to correspond closely with the 12° isotherm in most cases. Internal wave activity was observed during each run.

The thermocline, when internal waves are present, is a region of relatively high velocity shear combined with the large temperature gradient. Velocity shear due to internal waves could not be determined with any certainty because the internal wave velocities were only slightly higher than the noise level of the flowmeters. The maximum apparent shear was on the order of 1 cm $sec^{-1}m^{-1}$. The uncertainties in low velocity water motion measurements precluded estimation of the Richardson number.

Turbulent heat fluxes were calculated for six runs made at various depths. The array was positioned in each case such that the sensors were near and, in some cases, in the thermocline. As internal waves passed the array, the Lagrangian flow field was sampled to a vertical extent of

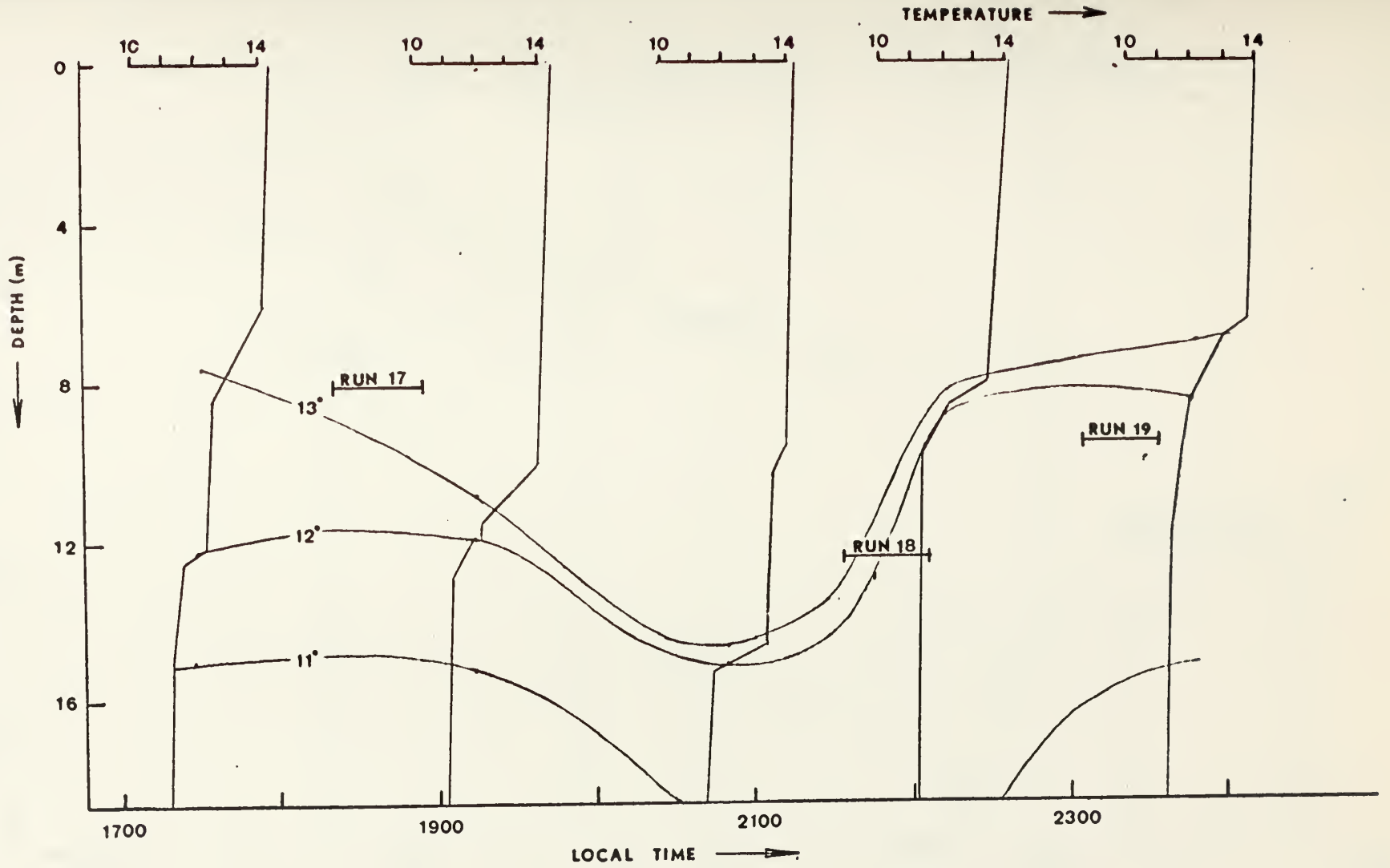

Figure 7a. Bathythermograph Traces for 24-26 April 1974 at the NUC Tower. Time of the Trace is Located at the 12°C Temperature Mark. Sensor Positions in Depth and Time are Included to Show the Position of the Sensors Relative to the Thermocline. The Gradients of Temperature are Based on Only the BT Samples and are not to be Construed as the Actual Mean Gradients Encountered by the Sensors During Each Run. (Figure continued on next page.)

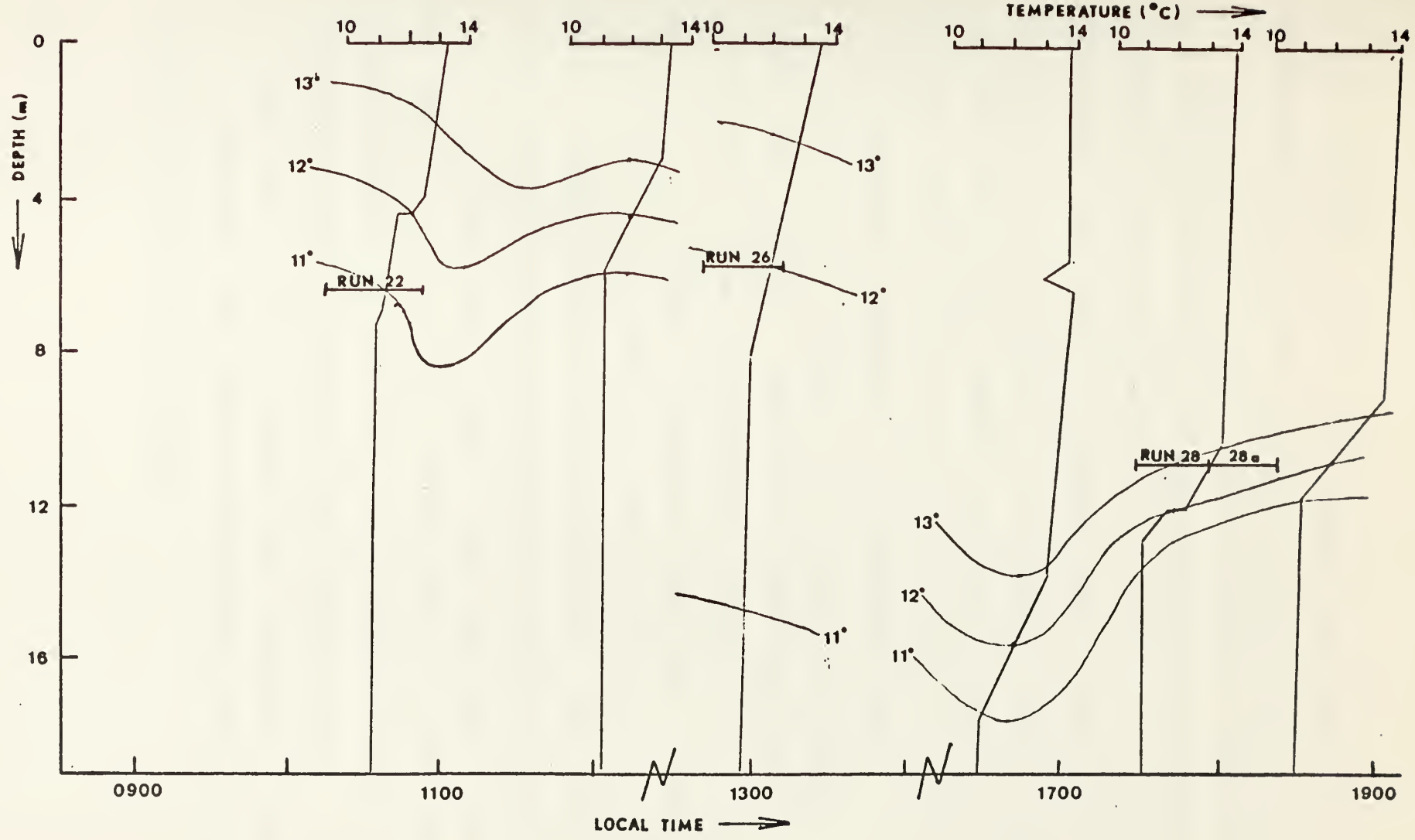
TEMPERATURE (°C)
10
14
DEPTH (m)
0
4
8
12
16
13°
12°
11°
RUN 22
RUN 26
RUN 28
28a
0900
1100
1300
1700
1900
LOCAL TIME

Figure 7b.

about 2-3 meters. Thus, the averages calculated from the experimental records were spatial as well as time averages.

The device of filtering out low frequency temperature and velocity data merely prevented internal wave components from biasing the measurements. Since available averaging times were insufficient to provide proper estimates at internal wave frequencies, it was decided to ignore them. Internal wave effects, however, were still observable in the filtered records because of the above mentioned sampling of the Lagrangian temperature and velocity fields.

The calculated turbulent heat fluxes were somewhat higher than expected. Advection of heat away from the experiment site was discounted as a reason for this result due to the low current velocities in the area. A counter-balancing flux contribution at the internal wave frequencies which had been filtered out was considered. The flux was calculated from unfiltered records but nothing conclusive could be observed due to lack of sufficient record length. The imposed vertical scale of twenty meters and the stable density gradient were presumed to limit turbulence to frequencies higher than that of the internal waves (Kitaigorodskii, 1973). Attention was subsequently focused on the extremely large effect of the surface waves on the temperature and velocity records.

VII. MEASURED HEAT FLUX

The heat flux measurements made from the NPS array were suspected of containing significant errors due to flowmeter misalignment. In light of the preceding error analysis it was considered possible to make certain corrections to the flux measurements if the tilt angle of the vertical velocity sensor were known. The cross spectrum between surface displacement and vertical velocity was available, and with the appropriate approximations, a relationship between the measured phase angle and the actual tilt angle was derived.

Several fortunate circumstances combined to allow the tilt angle to be calculated. The physical mounting of the flowmeters was such that rotation was possible only in the 1'-3' plane (referring to figure 6). In addition, coastal environments are usually characterized by relatively narrow banded wave direction spectra so the assumption could be made that the wave motions were essentially in one direction. Since the predominant wave direction was consistently within 30° of the azimuth of the plane of the 1'-3' flowmeter components, small angle approximations could be used. Referring again to figure 6, for small β_n, α_{33} can be considered equal to its projection on the 1-3 plane and the problem is simplified to that illustrated in figure 4, where

$\alpha_{33} = 90 - \alpha_{13}$.

The cross spectrum between wave displacement and vertical velocity for this situation is derived in Appendix B and can be written

$$2\int_0^\infty S_{\eta w}(f)\,df = 2\int_0^\infty (Co(f) - i\,Q(f))\,df =$$

$$= (\overline{\eta' w'} + \bar{\eta}\,\bar{U}\sin\alpha_{33}) - i(\bar{\eta}\,\bar{W}\cos\alpha_{33}) \qquad (32)$$

Making the assumption that random surface displacements (e.g. breaking wave crests) are essentially uncorrelated with turbulent velocities at a depth of 5 meters (the minimum measurement depth), or greater, allows the $\overline{\eta' w'}$ term to be neglected. The vertical integral scale, measured from temperature data to test this assumption, was 1.5 meters. The cross spectrum is now defined totally by wave-induced motions and the phase angle in the wave band is

$$\phi = \tan^{-1}\left(\frac{\int_{f_1}^{f_2} Q(f)\,df}{\int_{f_1}^{f_2} Co(f)\,df}\right)$$

$$= \frac{\bar{\eta}\,\bar{W}\cos\alpha_{33}}{\bar{\eta}\,\bar{U}\sin\alpha_{33}} \,. \qquad (33)$$

Solving for α_{33}:

$$\alpha_{33} = \tan^{-1}\left(\frac{\bar{W}}{\bar{U}\tan\phi}\right). \qquad (34)$$

The cross spectra between waves and vertical velocity were obtained for the two shallowest runs and α_{33} was calculated. The results are given in Table III.

Run 6: seas from 310T; swell from 290T

Run 10: seas from 300T; swell from 270T

vertical flowmeter	Run 6	Run 10
tilt angle (α_{33})	3.54°	3.62°

TABLE III. Tilt angle of vertical flowmeter axis. The azimuth of the plane of vertical and horizontal flowmeter components was 270T.

Using a value of α_{33} equal to 3.6 for all runs, equation (18) was used to calculate the wave-induced error and the correction was applied to the measured heat flux. The average temperature gradients during each run were also measured from thermistors approximately one half meter above and below the point of flux measurement. The eddy diffusion coefficient was then calculated from

$$K_H = \frac{\overline{\theta' w'}}{\partial \bar{\theta} / \partial z} \tag{35}$$

The turbulence correlation coefficient ($r'_{\theta w}$) was calculated from corrected values of $\overline{\theta' w'}$ and the turbulent intensities from Tables I and II. The results are given in Table IV. The turbulence correlation coefficients were all less than one except for run 26. A turbulence correlation coefficient greater than one indicates that there were errors in the

RUN #	17	18	19	22	26	28	28a
Local Time	1900	2200	2300	1000	1300	1800	1830
Measured Heat Flux $[\overline{\theta'*w'*}]$ [°C cm sec^{-1}]	-0.002	-0.007	-0.152	-0.333	-1.141	-0.040	-0.202
Corrected Heat Flux $[\overline{\theta'w'}]$ [°C cm sec^{-1}]	+0.085	+0.039	-0.116	-0.270	-1.051	-0.007	-0.133
Average Temperature Gradient $\frac{\partial\overline{\theta}}{\partial z}$ [°C - cm^{-1}]	0.004	0.004	0.002	0.008	0.015	0.002	0.012
Eddy Diffusion Coefficient, K_H [cm^2 sec^{-1}]	21.3	9.8	58.0	33.8	70.0	3.5	11.1
Turbulence Correlation Coefficient, $r'_{\theta w}$	0.19	0.13	0.88	0.95	2.77	0.08	0.80

TABLE IV. Turbulent Heat Flux $\frac{H}{\rho C_p} = \overline{\theta'w'}$ and Related Parameters Calculated from NPS Array Data and Corrected for Flowmeter Tilt. Averaging Time was 26 Minutes.

measurement which were not corrected for and, hence, run 26 is disregarded in the discussion below.

The variations of heat flux as internal waves pass a fixed sensor should reflect the variations in velocity and temperature gradients encountered. In the absence of large scale mixing events, such as the breaking of internal wave crests, the heat flux should be proportional to the temperature and velocity gradients. It was therefore expected that the measured heat flux would increase as the thermocline region was more extensively sampled. Figure 7 and Table IV show that this expectation was not fully realized, since a simple relationship between temperature gradient and heat flux was not observed.

Of the runs conducted at night (17, 18, 19), the first two indicated an upward transport of heat presumably due to convective overturn. Both these runs, although close to the thermocline, mainly sampled the isothermal regions above and below it. It was not immediately apparent why run 18, below the thermocline, would show an upward heat flux, because surface water would have had to be cooled quite radically to sink through the thermocline. The change in shape of the temperature profile before and after the run indicated that a large scale mixing event might have occured during the run, which would account for the upward heat flux. Run 19 sampled a region of relatively high temperature gradient which resulted in a net downward flux, as expected. The heat flux was less, however, than for a daytime run in a region of similar temperature gradient (run 28a).

Runs 22 and 28 were conducted during the late morning and afternoon, respectively. Run 22 sampled the thermocline extensively and there was evidence of a large scale mixing event, both in the temperature time series and in the BT samples. The heat flux was consequently large. Run 28 was divided into two runs because the first part of the run sampled an isothermal region while two very distinct internal wave troughs passed by the sensors during the second part of the run. There was no evidence of a large scale mixing event occuring at the level of the flux measuring sensors in run 28, although the thermistor placed a meter below did record a possible mixing event. This run was considered to be measuring only small scale turbulent flux at various distances from the thermocline.

The high turbulence correlation coefficients observed for runs 19, 22, and 28a correspond to relatively long periods of time during which the sensors were in the thermocline region. The inference can be made that gradient type eddy diffusion in this region is an efficient heat transport mechanism which can probably be closely approximated by a gradient diffusion model of the form of equation (35). The relationship between K_H and other thermocline parameters ($\partial\Theta/\partial z$, $\partial U/\partial z$) could not be determined because only two of the six runs (19, 28a) did not show evidence of larger scale mixing events.

On a qualitative basis,the results showed that small scale turbulent heat transport in the upper ocean is not

easily modeled. The mechanism for transfer seems to be a combination of gradient type diffusion and convection. Mixing at large scales is a factor and may be due to breaking of internal wave crests. It appears that large scale processes reestablish sharp temperature gradients which are again eroded by eddy diffusion and convection. Large increases in turbulent kinetic energy were not observed in the thermocline region, indicating that production of turbulence by internal wave-induced shear was not as important as production at the surface. The local Richardson number must therefore have been greater than the critical value of 0.25 for the maintenance of shear-induced turbulence.

VIII. CONCLUSIONS

Analysis of near surface velocity records in shallow water indicated that the ratio of turbulent to wave-induced kinetic energy was of order 10^{-1}. Because of the relatively large wave-induced fluctuations, large turbulent flux measurement errors can occur for small errors in directional response, phase response, or instrument alignment. Alignment errors are by far the most troublesome because they cannot be determined in the laboratory before measurements are made. Flowmeter misalignment of 3.6° caused errors in the calculated heat flux of about 25% to 100%. Momentum flux measurements would have been affected to a greater degree. It was shown how momentum flux measurements in the open ocean would be

less sensitive to misalignment errors than shallow water measurements. Deep water misalignment errors would be minimized by aligning the flowmeter axes as near as possible to the predominant direction of wave motion.

The heat flux measurements reported here were only an initial effort and the results could certainly be improved upon. Verification of the applicability of the gradient eddy diffusion model in the thermocline was not possible from the sparse data. It is felt that analysis of the remaining NUC tower runs will provide sufficient data to establish a relationship between the temperature and velocity structure in the thermocline and the eddy diffusivity.

APPENDIX A

The relative magnitudes of the wave-induced and turbulent fluctuations can be approximated by assuming that:

1.) the wave-induced and turbulent fluctuations are independent, and

2.) the wave-induced fluctuations can be described by linear wave theory.

Using the first assumption, the spectra of (1) are related according to:

$$S_u(f) = S_U(f) + S_{u'}(f) \qquad (a)$$

The second assumption allows $S_U(f)$ to be written in terms of the spectrum of the surface displacement ($S_\eta(f)$) as:

$$S_U(f) = |H^2(f)|\ S_\eta(f) \qquad (b)$$

where H(f) is a transfer function derived from linear theory. The coherence between U and η is given by

$$\gamma^2_{U\eta}(f) = \frac{\left|S_{U\eta}(f)\right|^2}{S_U(f)\ S_\eta(f)} \equiv 1 \qquad (c)$$

where the identity holds for a linear constant parameter system. Now

$$|S_{U\eta}(f)|^2 = S_U(f)\ S_\eta(f) \qquad (d)$$

and by assumption (1.)

$$|S_{U\eta}(f)|^2 = |S_{u\eta}(f)|^2 = S_U(f)\ S_\eta(f) \qquad (e)$$

The measured coherence between u and η is

$$\gamma^2_{u\eta}(f) = \frac{|S_{u\eta}(f)|^2}{S_u(f)\, S_\eta(f)} \qquad (f)$$

substituting (e) and (a),

$$\gamma^2_{u\eta}(f) = \frac{S_U(f)}{S_u(f)} = \frac{S_u(f) - S_{u'}(f)}{S_u(f)} \qquad (g)$$

which results in

$$S_{u'}(f) = S_u(f)\ (1 - \gamma^2_{u\eta}) \ .$$

APPENDIX B

1. Cross Spectrum Between Fourier Components of η and W*

$$\eta = \eta \sin \sigma t$$

$$W^* = U \sin \sigma t \cos \alpha_{13} + W \cos \sigma t \cos \alpha_{33}$$

$$= \tfrac{1}{2} U \sin(\sigma t + \alpha_{13}) + \tfrac{1}{2} U \sin(\sigma t - \alpha_{13})$$

$$- \tfrac{1}{2} W \cos(\sigma t - \alpha_{33}) + \tfrac{1}{2} W \cos(\sigma t + \alpha_{33})$$

$$R_{\eta w^*}(\tau) = \frac{1}{T}\int_0^T \Big[\tfrac{1}{2}\eta U \sin\sigma t \sin(\sigma t + \sigma\tau + \alpha_{13})$$

$$+ \tfrac{1}{2}\eta U \sin\sigma t \sin(\sigma t + \sigma\tau - \alpha_{13})$$

$$+ \tfrac{1}{2}\eta W \sin\sigma t \cos(\sigma t + \sigma\tau - \alpha_{33})$$

$$+ \tfrac{1}{2}\eta W \sin\sigma t \cos(\sigma t + \sigma\tau + \alpha_{33})\Big] \cdot dt$$

$$R_{\eta w^*}(\tau) = \tfrac{1}{2}\eta U \cos\alpha_{13} \cos(-\sigma\tau) + \tfrac{1}{2}\eta W \cos\alpha_{33} \sin(-\sigma\tau)$$

$$S_{\eta w^*}(f) \approx$$

$$\frac{1}{\tau_{max}}\int_0^{\tau_{max}} \Big\{ \tfrac{1}{2}\eta U \cos\alpha_{13} [\cos\sigma\tau \cos 2\pi f\tau - i \cos\sigma\tau \sin 2\pi f\tau]$$

$$- \tfrac{1}{2}\eta W \cos\alpha_{33} [\sin\sigma\tau \cos 2\pi f\tau - i \sin\sigma\tau \sin 2\pi f\tau] \Big\} \cdot d\tau$$

$$S_{\eta w^*}(f) \approx 0 \quad \text{if } f \neq 2\pi/\sigma$$

$$\approx \tfrac{1}{4}\eta U \cos\alpha_{13} + i\,\tfrac{1}{4}\eta W \cos\alpha_{33}$$

OTHERWISE.

2. Cross Spectrum Between Fourier Components of U* and W*.

$$U^* = U \sin\sigma t \cos\alpha_{11} + W \cos\sigma t \cos\alpha_{31}$$

$$W^* = U \sin\sigma t \cos\alpha_{13} + W \cos\sigma t \cos\alpha_{33}$$

$$U^* = \tfrac{1}{2} U \sin(\sigma t + \alpha_{11}) + \tfrac{1}{2} U \sin(\sigma t - \alpha_{11}) + \tfrac{1}{2} W \cos(\sigma t - \alpha_{31}) + \tfrac{1}{2} W \cos(\sigma t + \alpha_{31})$$

$$W^* = \tfrac{1}{2} U \sin(\sigma t + \alpha_{13}) + \tfrac{1}{2} U \sin(\sigma t - \alpha_{13}) + \tfrac{1}{2} W \cos(\sigma t - \alpha_{33}) + \tfrac{1}{2} W \cos(\sigma t + \alpha_{33})$$

$$\begin{aligned} R_{U^*U^*}(\tau) = \frac{1}{T}\int_0^T \Big[& \tfrac{1}{4} U^2 \sin(\sigma t + \alpha_{11}) \sin(\sigma t + \sigma\tau + \alpha_{13}) \\ & + \tfrac{1}{4} U^2 \sin(\sigma t + \alpha_{11}) \sin(\sigma t + \sigma\tau - \alpha_{13}) \\ & + \tfrac{1}{4} UW \sin(\sigma t + \alpha_{11}) \cos(\sigma t + \sigma\tau - \alpha_{33}) \\ & + \tfrac{1}{4} UW \sin(\sigma t + \alpha_{11}) \cos(\sigma t + \sigma\tau + \alpha_{33}) \\ & + \tfrac{1}{4} U^2 \sin(\sigma t - \alpha_{11}) \sin(\sigma t + \sigma\tau + \alpha_{13}) \\ & + \tfrac{1}{4} U^2 \sin(\sigma t - \alpha_{11}) \sin(\sigma t + \sigma\tau - \alpha_{13}) \\ & + \tfrac{1}{4} UW \sin(\sigma t - \alpha_{11}) \cos(\sigma t + \sigma\tau - \alpha_{33}) \\ & + \tfrac{1}{4} UW \sin(\sigma t - \alpha_{11}) \cos(\sigma t + \sigma\tau + \alpha_{33}) \\ & + \tfrac{1}{4} WU \cos(\sigma t - \alpha_{31}) \sin(\sigma t + \sigma\tau + \alpha_{13}) \\ & + \tfrac{1}{4} WU \cos(\sigma t - \alpha_{31}) \sin(\sigma t + \sigma\tau - \alpha_{13}) \\ & + \tfrac{1}{4} W^2 \cos(\sigma t - \alpha_{31}) \cos(\sigma t + \sigma\tau - \alpha_{33}) \\ & + \tfrac{1}{4} W^2 \cos(\sigma t - \alpha_{31}) \cos(\sigma t + \sigma\tau + \alpha_{33}) \\ & + \tfrac{1}{4} WU \cos(\sigma t + \alpha_{31}) \sin(\sigma t + \sigma\tau + \alpha_{13}) \\ & + \tfrac{1}{4} WU \cos(\sigma t + \alpha_{31}) \sin(\sigma t + \sigma\tau - \alpha_{13}) \\ & + \tfrac{1}{4} W^2 \cos(\sigma t + \alpha_{31}) \cos(\sigma t + \sigma\tau - \alpha_{33}) \\ & + \tfrac{1}{4} W^2 \cos(\sigma t + \alpha_{31}) \cos(\sigma t + \sigma\tau + \alpha_{33}) \Big] dt \end{aligned}$$

$$R_{u^*w^*}(\tau) =$$

$$\tfrac{1}{4} U^2 \cos(\alpha_{11}+\alpha_{13}) \cos\sigma\tau + \tfrac{1}{4} U^2 \cos(\alpha_{11}-\alpha_{13}) \cos\sigma\tau$$
$$- \tfrac{1}{4} UW \cos(\alpha_{11}+\alpha_{33}) \sin\sigma\tau - \tfrac{1}{4} UW \cos(\alpha_{11}-\alpha_{33}) \sin\sigma\tau$$
$$+ \tfrac{1}{4} UW \cos(\alpha_{31}+\alpha_{13}) \sin\sigma\tau + \tfrac{1}{4} UW \cos(\alpha_{31}-\alpha_{13}) \sin\sigma\tau$$

$$S_{u^*w^*}(f) = \tfrac{1}{8} U^2 \cos(\alpha_{11}+\alpha_{13}) + \tfrac{1}{8} U^2 \cos(\alpha_{11}-\alpha_{13})$$
$$+ \tfrac{1}{8} W^2 \cos(\alpha_{31}+\alpha_{33}) + \tfrac{1}{8} W^2 \cos(\alpha_{31}-\alpha_{33})$$
$$+ i\left[\tfrac{1}{8} UW \cos(\alpha_{11}+\alpha_{33}) + \tfrac{1}{8} UW \cos(\alpha_{11}-\alpha_{33})\right.$$
$$\left. - \tfrac{1}{8} UW \cos(\alpha_{31}+\alpha_{13}) - \tfrac{1}{8} UW \cos(\alpha_{31}-\alpha_{13})\right]$$

WHEN $f = \frac{2\pi}{\sigma}$; 0 OTHERWISE

$$S_{u^*w^*}(f) = \tfrac{1}{4} U^2 \cos\alpha_{11} \cos\alpha_{13} + \tfrac{1}{4} W^2 \cos\alpha_{31} \cos\alpha_{33}$$
$$+ i\left[\tfrac{1}{4} UW \cos\alpha_{11} \cos\alpha_{33} - \tfrac{1}{4} UW \cos\alpha_{31} \cos\alpha_{13}\right]$$

LIST OF REFERENCES

Bendat, K.R., and A.G. Piersol, 1971: Random Data: Analysis and Measurement Procedures, Whiley-Interscience.

Bowden, K.F., and M.R. Howe, 1963: "Observations of Turbulence in a Tidal Current," J. Fluid Mech. 17, 271-84.

Hagen, J.B., 1974: "Acoustic Fluctuations Due to Shallow Water Thermal Microstructure," M.S. Thesis, Naval Postgraduate School, September, 1974.

Kaiser, J.A.C., and K.G. Williams, 1974: "Measurements of the Vertical Heat Flux in the Upper Ocean Layer," J. Phys. Oceanogr., 4:2, 137-44.

Kinsman, B., 1965: Wind Waves, Prentice-Hall.

Kitaigorodskii, S.A., 1971: The Physics of Air-Sea Interaction, English Translation, U.S. Dept. of Commerce, Washington, D.C.

Kitaigorodskii, S.A., Y.Z. Miropolskii, and B.N. Filyushin, 1973: "Use of Ocean Temperature Fluctuation Data to Distinguish Internal Waves from Turbulence," Isv., Atmos. Oceanic Phys., 9:3, 272-292.

National Oceanographic Instrumentation Center (NOIC), 1974: Technical Bulletin RN 1009, Washington, D.C.

Phillips, O.M., 1966: Dynamics of the Upper Ocean, Cambridge University Press.

Seitz, R.C., 1971: "Measurement of a Three-Dimensional Field of Water Velocities at a Depth of One Meter in an Estuary," J. Mar. Res., 29:2, 140-150.

Tennekes, H., and J.L. Lumley, 1972: A First Course in Turbulence, MIT Press.

Thornton, E.B., and N.E.J. Boston, 1974: "Separating Turbulent and Wave-Induced Velocity and Temperature Fluctuations," J. Geophys. Res.

Voskanyan, A.G., A.A. Pivovarov, and G.G. Khundzhua, 1969: "Experimental Studies of the Thermal Structure and Turbulent Heat Exchange in the Surface Layer of the Sea," Oceanology, 10:4, 449-56.

Williams, R.B., and C.H. Gibson, 1974: "Direct Measurements of Turbulence in the Pacific Equatorial Undercurrent,: J. Phys. Oceanogr., 4:1, 104-108.

Yefimov, V.V., and G.N. Khristoforov, 1971: "Spectra and Statistical Relations Between the Velocity Fluctuations in the Upper Layer of the Sea and Surface Waves," Isv. Atmos. Oceanic Phys., 7:12, 1290-1310.

Yefimov, V.V., and G.N. Khristoforov, 1972: "Dynamics of Surface Waves with Allowance for the Turbulent Nature of the Motion," Isv. Atmos. Oceanic Phys., 8:1, 52-66.

INITIAL DISTRIBUTION LIST

		No. Copies
1.	Defense Documentation Center Cameron Station Alexandria, Virginia 22314	2
2.	Library (Code 0212) Naval Postgraduate School Monterey, California 93940	2
3.	Department of Oceanography, Code 58 Naval Postgraduate School Monterey, California 93940	3
4.	Oceanographer of the Navy Hoffman Building No. 2 200 Stovall Street Alexandria, Virginia 22332	1
5.	Office of Naval Research Code 480 Arlington, Virginia 22217	1
6.	Dr. Robert E. Stevenson Scientific Liaison Office, ONR Scripps Institution of Oceanography La Jolla, California 92037	1
7.	Library, Code 3330 Naval Oceanographic Office Washington, D.C. 20373	1
8.	SIO Library University of California, San Diego P.O. Box 2367 La Jolla, California 92037	1
9.	Department of Oceanography Library University of Washington Seattle, Washington 98105	1
10.	Deaprtment of Oceanography Library Oregon State University Corvallis, Oregon 97331	1
11.	Commanding Officer Fleet Numerical Weather Central Monterey, California 93940	1

12. Commanding Officer — 1
Environmental Prediction Research Facility
Monterey, California 93940

13. Department of the Navy — 1
Commander Oceanographic System Pacific
Box 1390
FPO San Francisco 96610

14. Dr. Clayton Paulson — 1
Department of Oceanography
Oregon State University
Corvallis, Oregon 97331

15. Dr. J. Duncan Smith — 1
Department of Oceanography
University of Washington
Seattle, Washington 98195

16. Dr. E. B. Thornton — 1
Department of Oceanography
Naval Postgraduate School
Monterey, California 93940

17. LT J. B. Hagen — 1
USS Benjamin Franklin SSBN 640 (Gold)
FPO New York 09501

18. LT G. K. Nifontoff — 1
717 Tenth Street
Coronado, California 92118

Thesis
N584
c.1

Nifontoff
Analysis of wave-induced errors in turbulent flux measurements.